## LANGMUIR

pubs.acs.org/Langmuir Article

### Rate, Efficiency, and Mechanisms of Electrochemical Perfluorooctanoic Acid Degradation with Boron-Doped Diamond and Plasma Electrodes

Necip B. Üner, Paola Baldaguez Medina, Jasmine L. Dinari, Xiao Su,\* and R. Mohan Sankaran\*



Cite This: Langmuir 2022, 38, 8975-8986



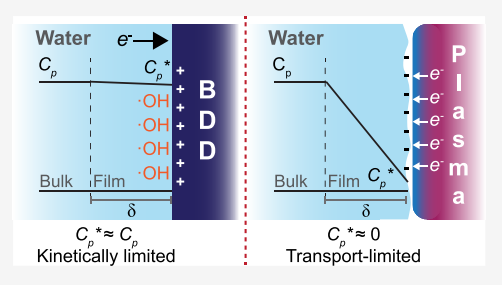
**ACCESS** I

Metrics & More

Article Recommendations

Supporting Information

ABSTRACT: The removal of per- or polyfluorinated alkyl substances (PFAS) has received increasing attention because of their extreme stability, our increasing awareness of their toxicity at even low levels, and scientific challenges for traditional treatment methods such as separation by activated carbon or destruction by advanced oxidation processes. Here, we performed a direct and systematic comparison of two electrified approaches that have recently shown promise for effective degradation of PFAS: plasma and conventional electrochemical degradation. We tailored a reactor configuration where one of the electrodes could be a plasma or a boron-doped diamond (BDD) electrode and operated both electrodes galvanostatically by continuous direct current. We show that while both



methods achieved near-complete degradation of PFAS, the plasma was only effective as the cathode, whereas the BDD was only effective as the anode. Compared to the BDD, plasma required more than an order of magnitude higher voltage but lower current to achieve similar degradation efficiency with more rapid degradation kinetics. All these factors considered, it was noted that plasma or BDD degradation resulted in similar energy efficiencies. The BDD electrode exhibited zero-order kinetics, and thus, PFAS degradation using the conventional electrochemical method was kinetically controlled. On the contrary, analysis using a film model indicated that the plasma degradation kinetics of PFAS using plasma were mass-transfer-controlled because of the fast reaction kinetics. With the help of a simple quantitative model that incorporates mass transport, interfacial reaction, and surface accumulation, we propose that the degradation reaction kinetically follows an Eley–Rideal-type mechanism for the plasma electrode, and an intrinsic rate constant of  $2.89 \times 10^8 \,\mathrm{m}^4 \,\mathrm{mol}^{-1} \,\mathrm{s}^{-1}$  was obtained accordingly. The investigation shows that to realize the true kinetic potential of plasma degradation for water treatment, mass transfer to the interface must be enhanced.

#### INTRODUCTION

The widespread use of per- or polyfluorinated alkyl substances (PFAS) in many commercial, industrial, and firefighting applications has led to their contamination of water supplies, including wastewater, groundwater, and even drinking water. Many PFAS are suspected to be carcinogenic, genotoxic, or cytotoxic<sup>1-4</sup> and can be retained in both the environment and biota for very long times,<sup>5</sup> due to their chemical stability that stems from the C–F bonds (~5 eV).<sup>6</sup> In wastewater streams in urban centers, the concentration of PFAS is commonly found above the regulation limits,<sup>7</sup> and classical advanced oxidation processes, such as treatment with Fenton's reagent and UV light exposure, have encountered challenges in degrading PFAS.<sup>8,9</sup> Therefore, there have been intense recent efforts to develop new approaches to remove PFAS more effectively and efficiently.<sup>10,11</sup>

Over the last 20 years, researchers have proposed many methods to remove PFAS, and these methods can be divided into ones that focus either on separation or degradation. Examples of separation-based methods include adsorption, 12-14 ion exchange, 15,16 membrane separation, 17,18 and foam fractionation. More recently, electrosorption-based

technologies have demonstrated potential for selectively removing PFAS through functional surfaces. <sup>22–24</sup> Although these methods can physically remove PFAS from water, the PFAS ultimately remains as a persistent waste that needs to be chemically degraded. Examples of degradation-based methods include sonolysis, <sup>8,25,26</sup> photochemical, <sup>27–29</sup> electrochemical, <sup>27–29</sup> and plasma <sup>43–52</sup> processes. In the last decade, electrochemical and plasma-based processes have attracted much attention because of their capability to mineralize PFAS into F<sup>-</sup> and CO<sub>2</sub>. <sup>45</sup> The two approaches bear interesting similarities and differences. Both use electricity as an input and promote chemical reduction and oxidation reactions. However, plasmas require a much higher voltage to initiate and sustain gas breakdown, and there are different chemical species produced because of the complex nonequilibrium chemistry.

**Received:** May 13, 2022 **Revised:** June 28, 2022 **Published:** July 15, 2022





Figure 1. Schematic of experimental setup and electrodes. (a) Schematic of electrochemical cell. CE and WE stand for the counter and working electrodes, respectively. (b,c) Schematic of working electrodes, BDD and the plasma.  $R_{\rm B}$  is the ballast resistor, and  $R_{\rm T}$  is the test resistor where the current is measured. HV stands for high voltage. (d) False-color snapshots of the plasma cathode operated at the surface of a stirred PFOA solution at 2 mA. The snapshots were obtained with a digital microscope with no external light. The scale bar corresponds to 0.5 mm, and the magnification is the same for all four panels. The dashed line and the arrow on each panel indicate the changing water level due to stirring.

In a limited number of reports, it was shown that plasmas were highly suitable for the degradation of surface-active chemicals, 53 such as PFAS, and it was argued that plasma-based methods are more energy-efficient than classical electrochemical oxidation for PFAS degradation. 45,50 However, a comprehensive comparison of the kinetics, energy efficiencies, and mechanisms associated with PFAS degradation between plasma and electrochemical treatment remains absent. Fundamentally, such a study would reveal the different reaction pathways accessible by either approach. Technologically, the study would show which process has advantages or disadvantages for implementation, or if it is possible to combine them in synergistic ways. A natural obstacle is how these two somewhat distinct approaches can be compared in a meaningful way (i.e., "apples-to-apples"), which would necessitate careful consideration of electrochemical setup, polarities, and operating conditions.

Here, we present a direct and systematic comparison of a plasma and a conventional electrochemical process for PFAS degradation by using a basic galvanostatically operated reactor configuration in which one of the electrodes was a plasma or a boron-doped diamond (BDD) electrode, serving either as the cathode or the anode. A BDD electrode was chosen as the conventional electrode since it is known to be corrosionresistant<sup>54</sup> and stable at high current densities.<sup>55</sup> Furthermore, it has a wide potential window<sup>56</sup> and a high overpotential for O<sub>2</sub> generation,<sup>57</sup> thereby constituting the state-of-the-art electrode for the oxidation of PFAS.<sup>7,32-35,38-41</sup> Both BDD and plasma electrodes were used in the same cell under the same mixing conditions, and the currents employed were comparable. Long-chain, surface-active PFAS molecules are especially prevalent contaminants; therefore, perfluorooctanoic acid (PFOA) was selected as the model PFAS compound. The effect of polarity, kinetics, and energy efficiencies were assessed for both electrodes. Split cell and radical scavenger experiments provided mechanistic insight that the plasma electrode operates in a vastly different manner than the BDD electrode but surprisingly similar in terms of energy efficiency.

#### EXPERIMENTAL METHODS

**Electrochemical Experiments.** In most experiments, a 66.6 mm wide, 250 mL single-compartment borosilicate cell (Adams & Chittenden), with a gas-tight Teflon lid and feedthroughs for the electrodes, a sparging tube, and the exhaust, was used (Figure 1a), unless otherwise specified. A BDD electrode or a pin-to-plane plasma

electrode was inserted into the cell and served as the working electrode. Both electrodes allowed argon (Ar UHP300, Airgas) to flow into the cell at a rate of 100 sccm regulated by a mass flow controller (MC Series, Alicat). Unless otherwise noted, the counter electrode was a platinum-coated Ti mesh (Part #592777, Fuel Cell Store). All experiments were conducted under an Ar atmosphere.

The BDD electrode was a commercially available 10  $\mu$ m thick BDD layer on a doped silicon substrate (0040004036, IKA). The electrode was electrically connected to a nickel/chromium wire using conductive carbon glue (16050, Ted Pella), resulting in negligible resistance when compared to the ohmic resistances of the electrolytes used in this study (Figure 1b). The electrode was connected to a direct-current (DC) power supply (Model 9206, B&K Precision), and the current density was fixed at 20 mA/cm², as measured by the supply. The immersed area was approximately 0.5 cm² (10 mA total current).

The plasma electrode was comprised of a stainless-steel needle (RS-6066, Roboz) and a fused silica tube that surrounded the needle to introduce a sheath gas flow (Figure 1c). The needle had a diameter of 0.5 mm, and the radius of curvature at the tip was approximately 0.1 mm. The tip of the needle was placed 1.25 mm above the liquid surface measured with a digital microscope (Edge AM4115ZTL, Dino-Lite). The fused silica tube had an inner diameter of 4 mm and an outer diameter of 6.4 mm, and it was placed approximately 3 mm above the liquid surface. The needle was biased with high voltage to generate a plasma by a DC power supply with switchable polarity (Series 230, Bertan). The breakdown voltage was  $2.0 \pm 0.2$  kV. The current was limited with a 651  $\ensuremath{k\Omega}$  ballast resistor and measured with a 512  $\Omega$  test resistor, both in series, and the voltage between the plasma and counter electrodes was measured with a high voltage probe (80K-40, Fluke). The plasma was a dynamic DC glow discharge that adapted to the moving water surface (vide infra) beneath it (Figure 1d). The current was varied between 0.55 and 4 mA, and it was stable within  $\pm 20 \,\mu\text{A}$  of the set current value throughout all treatment times.

All experiments were conducted with a 20 mL solution composed of deionized water (HPLC grade, AH365, Honeywell), 20  $\mu$ M PFOA (95%, Sigma Aldrich), and 20 mM NaCl (>99.5%, Millipore Sigma) as the electrolyte unless otherwise noted. Before every experiment, the solution was sparged with 100 sccm Ar for 5 min, and the headspace of the cell was purged with 500 sccm Ar for 10 min. During sparging, purging, and the degradation experiments, the liquid was rigorously mixed at approximately 400 rpm with a large magnetic stirrer (3/4"  $\times$  1/4"  $\times$  1/4",  $L\times W\times H$ ). A limited number of experiments were carried out in a gas-tight split cell with a cation exchange membrane (SELEMION, AGC Seimi Chemicals Co.), under the same operating conditions.

**Scavenger Experiments.** Solvated electron scavenging experiments were conducted by adding NaNO<sub>3</sub> (>99.0%, Millipore Sigma), and OH radical scavenging experiments were conducted by adding disodium terephthalate (NaTA, >99.0%, Alfa Aesar) to the PFOA

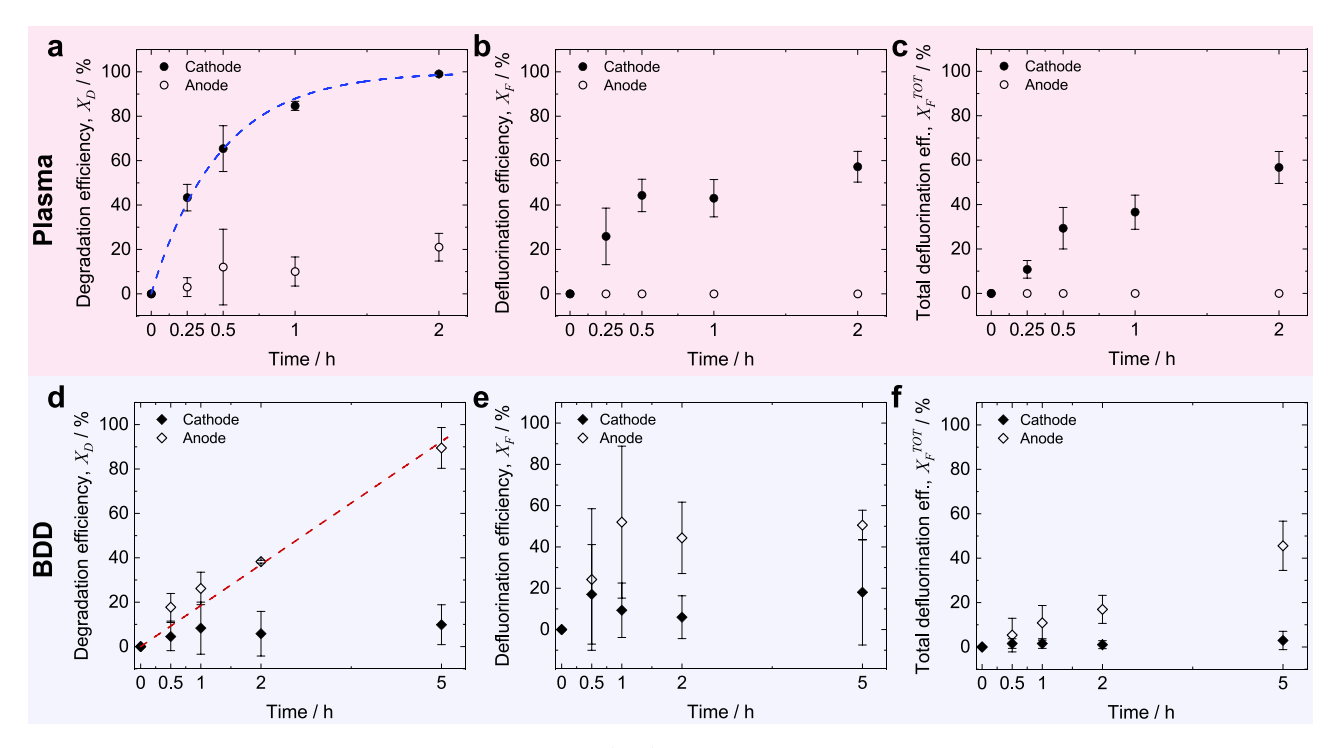


Figure 2. Efficiencies of PFOA degradation and defluorination. (a–c) Degradation, defluorination, and total defluorination efficiencies for the plasma electrode. The current was 2 mA. (d–f) Degradation, defluorination, and total defluorination efficiencies for the BDD electrode. The current was 10 mA, and the current density was 20 mA/cm $^2$ . The blue and red dashed lines for the plasma and the BDD degradation efficiencies are first- and zero-order fits, respectively.

solution with concentrations ranging from 20 to 120 mM. The hydroxylation product of NaTA, 2-hydroxyterephthalic acid (HTA), was quantified fluorometrically using a microplate reader (SpectraMax iD3, Molecular Devices). The excitation wavelength was 310 nm, and the emission wavelength was 425 nm. Calibration was done by using a stock solution of 0.5 mM HTA (>95%, TCI America) in deionized water (Figure S1).

**Detection of PFOA and Fluoride.** To detect the remaining concentration of the anionic PFOA in solution after degradation, a liquid chromatography-mass spectrometry (LC–MS) system with electrospray ionization was employed. A Waters Synapt G2Si with a Waters Acquity H-class UPLC system was employed, with a Waters ACQUITY UPLC BEH C18 column (1.7  $\mu$ m, 2.1 mm × 50 mm) and MassLynx 4.1 software for data processing. The column temperature was kept at 40 °C, and the flow rate was maintained at 0.4 mL/min. Also, 5 mM ammonium acetate solution was used as mobile phase A and acetonitrile as mobile phase B. Each run contained an injection volume of 0.5  $\mu$ L of a solution that consisted of a maximum concentration of 1  $\mu$ M PFOA and was performed in a gradient elution mode (Table S1) using negative ionization. A new calibration curve was obtained before each analysis.

To measure fluoride removed from PFOA by degradation, a Thermo Fisher Dionex 2100 ion chromatography instrument equipped with an EGC III KOH eluent generator, which contained a conductivity cell, a pump, an AS-AP autosampler, and a column capable of separating the fluoride species, a Dionex IonPac AS18 (4  $\times$  250 mm) anion exchange column with an in-line AG18 guard (4  $\times$  50 mm), was utilized. In order to lower the background eluent, a Thermo Scientific ADRS 600 4 mm suppressor was used. All samples were filtered through a 0.22  $\mu$ m PTFE membrane syringe filter (Biomed Scientific) without further dilution. Standard solutions were prepared from a fluoride standard (1000 mg/L, Sigma Aldrich) and diluted using deionized water produced with a Milli-Q system. A calibration curve was run before each experiment. Results were analyzed using Chromeleon v6.8 software.

**Figures of Merit.** From the measured concentrations of PFOA and fluoride after treatment, it was possible to assess the performance

of the electrodes with respect to removing PFOA from the solution. The three following figures of merit, which are commonly used in the literature for PFOA degradation, were calculated. The first is the degradation efficiency,  $X_{\rm D}$ , which is the percentage conversion of PFOA into any other chemical:

$$X_{\rm D} = \left(1 - \frac{C_{\rm p}}{C_{\rm p0}}\right) \cdot 100 \tag{1}$$

where  $C_p$  is the concentration of PFOA after treatment and  $C_{p0}$  is the initial concentration. The second is the defluorination efficiency,  $X_p$ , which is the percentage of fluoride extracted from the amount of PFOA degraded:

$$X_{\rm F} = \left[ \frac{C_{\rm F}}{15(C_{\rm p0} - C_{\rm p})} \right] \cdot 100 \tag{2}$$

with  $C_F$  being the concentration of fluoride. The third and last is the total defluorination efficiency,  $X_F^{\rm TOT}$ , which is the theoretical maximum percentage of fluoride that can be extracted from the initial amount of PFOA:

$$X_{\rm F}^{\rm TOT} = \frac{X_{\rm D}X_{\rm F}}{100} = \frac{C_{\rm F}}{15C_{\rm p0}} \cdot 100$$
 (3)

#### ■ RESULTS AND DISCUSSION

**Degradation Kinetics of PFOA.** We initially evaluated the degradation and defluorination of PFOA as a function of time in separate experiments with a BDD or plasma electrode serving as the cathode or anode (Figure 2). The polarity was observed to substantially affect the degradation rate and defluorination efficiencies for both the BDD and plasma electrodes. Operating the plasma as the cathode rapidly degraded PFOA and almost completely removed it within 2 h of treatment, whereas operating as the anode was much slower

(Figure 2a). Interestingly, an anodic plasma was completely ineffective in defluorinating PFOA (Figure 2b,c). An Ar plasma comprises negatively charged electrons and positively charged gas ions, in addition to other neutral species. When operated as the anode, the ions are accelerated toward the plasma-water interface, and when operated as the cathode, the electrons are accelerated. Ions, because of their much higher mass, could presumably induce carbon chain breakage through their relatively large collisional momentum/energy transfer or withdraw an electron from a PFOA anion nearby the surface through charge neutralization, leading to Kolbe decarbox-ylation of the resulting PFOA radical. 37,40,50,58 These processes could lead to a small amount of PFOA degradation (Figure 2a) but do not result in cleavage of the C-F bonds involved; hence, there is no defluorination (Figure 2b,c). In contrast, a cathodic plasma rapidly generates free fluoride up to 60%  $X_{\rm F}^{\rm TOT}$ , suggesting that gas-phase electrons and any potential chemistry they induce at the interface are more effective in degrading and defluorinating PFOA.

Polarity-wise, the BDD electrode was found to work in a complete opposite way in comparison to the plasma electrode. Unlike the plasma, cathodic operation led to insignificant degradation and defluorination (Figure 2d-f). However, an anodic BDD was much more effective in degrading and defluorinating PFOA. Anodic operation is the common configuration used in electrochemical degradation of perfluorinated surfactants, 7,32-36,38-41 likely due to the favorable oxidation characteristics of the hydrophilic segments of these molecules.<sup>59</sup> Previous studies indicated that at high potentials, such as the values used in this study (vide infra), the active sites on the BDD can participate in direct electron transfer and physisorbed OH generation, which lead to oxidation of organic contaminants.  $^{60,61}$  With the BDD, PFOA was degraded linearly in time, whereas defluorination happened more irregularly (Figure 2e). Nevertheless, when  $X_F^{TOT}$  was calculated via eq 3, a linearly increasing trend was obtained, akin to  $X_{\rm D}$  in this configuration (Figure 2f). The anodic BDD removed almost all of the PFOA in 5 h and eventually had a  $X_{\rm F}^{\rm TOT}$  value around 50%, slightly less than that of the plasma cathode.

The anodic BDD and cathodic plasma were found to display different types of degradation kinetics. As can be seen from the fits in Figure 2a, the cathodic plasma exhibited first-order-like kinetics (Figure S3), whereas degradation by anodic BDD was zero-order (Figure 2d). First-order kinetics for plasma-induced degradation of PFAS are consistent with many previous reports in the literature. <sup>43–51</sup> For an anodic BDD, first-order kinetics for PFAS degradation have been previously reported, 7,32-35,38-41 unless mass transfer limitations were overcome by, for example, using a rotating disk electrode setup<sup>62,63</sup> in which case the kinetics were zero order. In our case, rigorous stirring caused local velocities between 26 and 40 cm/s near the BDD electrode, as estimated from the tangential velocity of the stir bar at 400 RPM. Furthermore, the immersion depth of the electrode was low (0.5 cm<sup>2</sup>), and the current density was high (20 mA/cm<sup>2</sup>). All these factors increase the possibility of enhancing mass transfer and saturating the active sites that play a role in PFOA degradation, subsequently leading to a reaction-controlled process.

Energy Efficiency Comparison between BDD and Plasma Treatment. We next compared the energy efficiencies of the two electrodes in their optimal configurations (anodic BDD and cathodic plasma). Since both

electrodes treated the same amount of PFOA in the same cell and with the same mixing conditions, plotting  $X_D$  as a function of the energy spent during degradation directly compares the energy efficiency of the BDD and the plasma (Figure 3). In the

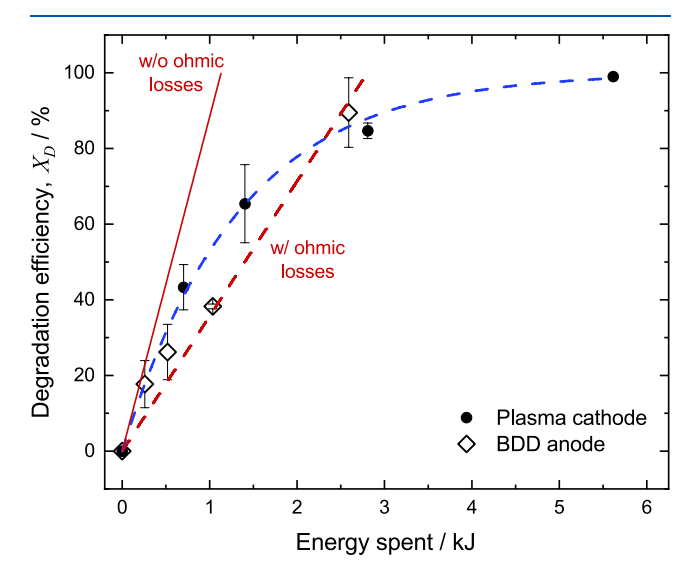


**Figure 3.** Energy spent during plasma and electrochemical degradation. Data and fits presented in Figure 2a,d are reproduced, with the x axis being the energy spent during degradation. The solid red line is the energy used for a hypothetical cell with insignificant ohmic losses.

case of the plasma, the cell voltage was 390 V at 2 mA (Figure S2), much higher than the cell voltage measured for the BDD, which was 14.4 V. However, since degradation kinetics are faster with the plasma, similar energy consumption was found for both electrodes at 85% degradation. For the initial degradation period, e.g., short times and low total energy spent, the plasma is more efficient than the BDD. However, as the PFOA concentration decreases, the energy efficiency of the plasma decreases significantly. We infer that at lower PFOA concentrations, the mass transfer rate to the plasma-liquid interface where the reaction occurs is low, and concomitantly, the degradation rate is low. The first half of the total energy spent by the plasma degrades PFOA by 85%, and the remaining half degrades it by only 10%. These observations indicate that the plasma could be highly efficient for degrading concentrated contaminant solutions where the mass transfer rate of PFAS to the plasma-liquid interface is high.

The BDD was found to be as efficient as the plasma at high PFOA concentrations, as can be seen from the overlapping trends in Figure 3, if ohmic losses were removed. The ohmic losses for the electrolyte solution that surrounds the electrodes were estimated via the finite element method to be 60% of the total power input (Figure S4). This calculation indicates that decreasing the distance between the working and counter electrodes could significantly increase the energy efficiency. However, a smaller distance would also decrease the potential between the electrodes under galvanostatic conditions, resulting in lower defluorination rates, 30 which depends on direct electron transfer.

The performance of the BDD and the plasma electrodes employed in this study compared well with other electrochemical and plasma-based approaches in the literature (Tables S2 and S3). Many performance metrics have been used to gauge the energy efficiency of the PFAS degradation

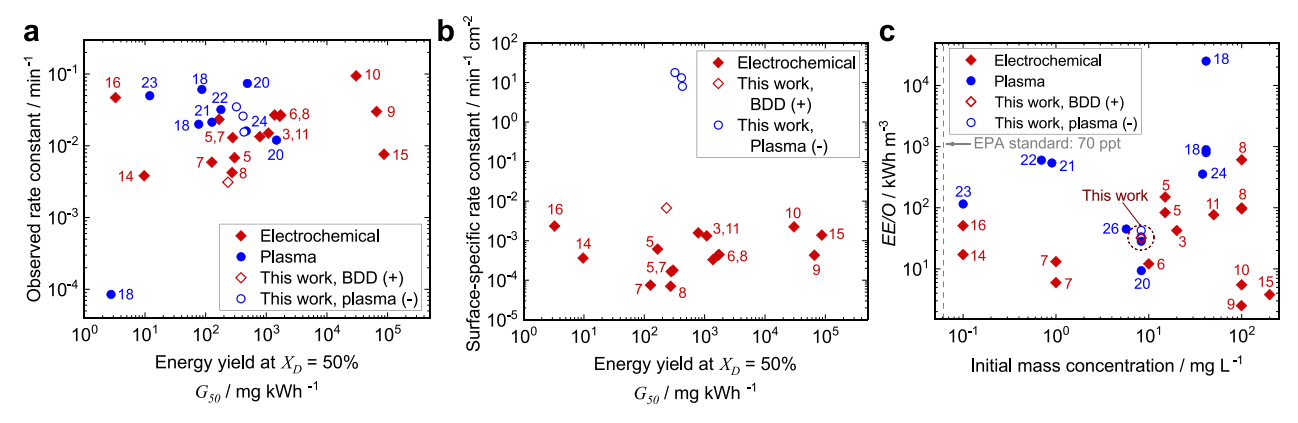


**Figure 4.** Comparison of performance metrics for PFOA degradation with the literature. (a) Observed rate constant as a function of  $G_{50}$ , the specific energy consumption at 50% degradation efficiency. (b) Surface-specific rate constant as a function of  $G_{50}$ . (c) Electric energy per order, EE/O, parameter as a function of initial PFOA concentration. The results obtained in this work are given for three different currents: 0.55, 1, and 2 mA from top to bottom in panels a and b, respectively. Details for the references that are indicated by numbering are provided in the Supplementary Information, Tables S2 and S3, along with the parameters used to calculate the performance metrics.

processes, and in this work, three of them were chosen to provide a comprehensive assessment. Namely, these metrics were the observed rate constant,  $k_{\text{obs}}$ , the energy yield for 50% degradation efficiency, abbreviated as  $G_{50}$ , and the electric energy per order parameter, EE/O, which is the energy cost for decreasing the PFAS concentration by an order of magnitude (Figure 4). We note that  $G_{50}$  and EE/O differ from each other since  $G_{50}$  is dependent on the initial PFOA concentration, whereas EE/O is not. A detailed description of the formulations of these metrics for both first- and zero-order reactions is given in the Supplementary Information. Previous electrochemical studies generally reported lower rate constants when compared to plasma-based degradation processes, but the highest energy efficiencies, i.e., highest  $G_{50}$  values, were achieved with BDDs serving as the anode (Figure 4a). While the  $G_{50}$  of the plasma electrode used in this work compared favorably, the  $k_{\rm obs}$  of the BDD electrode was found to be lower than literature values. In Figure 4b, we also show the surfacespecific  $k_{\text{obs}}$ , which is  $k_{\text{obs}}$  divided by the immersed electrode area, which was found to be among the highest reported for BDD and dimensionally stable mixed-oxide anodes. Therefore, the low overall  $k_{obs}$  value of our BDD-based degradation process most probably resulted from the low immersed area of the electrode (see Table S2 for literature values). Our goal was not necessarily to optimize the operation of the BDD for PFAS degradation, but rather to compare with the plasma electrode under as similar conditions as possible, including the reaction area. Assuming that the cathodic plasma degradation process can be approximated as a surface reaction predominantly happening at the plasma-liquid interface due to the low penetration depths of electrons, 64,65 we were able to also estimate the surface-specific rate constant of the plasma degradation process. Since the plasma electrode was operated continuously, the interfacial area was relatively easy to measure,  $\sim 0.2 \text{ mm}^2$ . Such a small area, when combined with a large rate constant (Figure 4a), results in very large surfacespecific rate constants, which are at least 3 orders of magnitude larger than that of the BDD (Figure 4b). As for the EE/O parameter, considering the order of the initial PFOA concentration used in this work, the obtained values were low when compared to literature results. Since the same amounts of volume were treated by the BDD and plasma electrodes and the energy consumptions were similar, it is not

so surprising that the EE/O values were also similar (Figure 3). Overall, for two distinctly different types of electrodes operating at opposite polarities that undoubtedly lead to different mechanisms for PFOA degradation, the similarity of the  $G_{50}$  and EE/O values is unexpected and possibly just coincidental. Additional experiments and analysis aimed at the kinetics and mechanistic aspects are necessary to further unravel how these electrodes fundamentally operate for PFAS degradation.

Remarkably, the  $k_{\rm obs}$  values for the plasma electrodes from the literature and in this work were found to fall within an order of magnitude range, despite having vastly different operation modes, powers, and excitation frequencies, as can be seen in Figure 4a. With our plasma electrode, decreasing the current shifted  $G_{50}$  to higher values (Figure 4a), indicating that more energy was wasted at higher currents, i.e., decreasing energy efficiency with higher currents. Combined with the exceedingly high values of the surface-specific reaction rate constant for the plasma electrode, these observations suggest that plasma-based degradation processes are severely mass transfer-limited.

Mass Transfer and Reaction Kinetic Analysis for **PFOA Degradation.** The observed rate constants presented in Figure 4 could be related to mass transfer, chemical kinetics, or some combination of both. Additional experiments are usually required to elucidate the contributions of mass transfer and kinetics to the observed degradation rate, and in cases where complete mass transfer or kinetic control is not easily achievable, a reaction-diffusion model with a predefined rate expression is needed to obtain quantitative estimates of the mass transfer coefficient and the intrinsic reaction rate constant. The simplest relevant model for combined mass transfer and interfacial chemical kinetics in our system is a film model<sup>66</sup> (see Figure S5 and the related section in the Supplementary Information for a review of the model). For zero-order kinetics, the model yields an expression for degradation efficiency that does not depend on the mass transfer coefficient,  $k_{\rm m}$ ; i.e., degradation is kinetically controlled:

$$\frac{X_{\rm D,0}}{100} = \frac{A_{\rm s}}{V_{\rm liq}C_{\rm p0}}k_{\rm r,0}t\tag{4}$$

where  $A_{\rm s}$  is the interfacial area for treatment,  $V_{\rm liq}$  is the liquid bulk volume, and  $k_{\rm r,0}$  is the intrinsic reaction rate constant for zero-order reaction on the surface. For the BDD electrode,  $A_{\rm s}$  is equal to the immersed electrode area, and  $k_{\rm r,0}$  has units of moles per unit time per electrode area. The linear increase in  $X_{\rm D,0}$  replicates the experimental results shown in Figure 2d, and  $k_{\rm r,0}$  is found to have a value of  $4.7 \times 10^{-7}$  mol/m²s.

For first-order degradation kinetics at the interface, the film model yields the following expression for degradation efficiency:

$$\frac{X_{\rm D,1}}{100} = 1 - \exp\left(-\frac{A_{\rm s}}{V_{\rm liq}} \frac{k_{\rm r,1}}{1 + k_{\rm r,1}/k_{\rm m}} t\right) \tag{5}$$

Eq 5 is suitable for describing degradation with the plasma electrode, since it gives an exponential trend for  $X_D$ , just like the exponential fit shown in Figure 2a for plasma degradation. From eq 5,  $k_{\text{obs},1}$ , the first-order observed rate constant shown in Figure 4a, can be defined as

$$k_{\text{obs,1}} = \frac{A_{\text{s}}}{V_{\text{liq}}} \frac{k_{\text{r,1}}}{1 + k_{\text{r,1}}/k_{\text{m}}} \tag{6}$$

It is important to note that in eqs 5 and 6, it is not clear whether  $k_{r,1}$  is the intrinsic rate constant since one would derive an equation that is exactly the same as eq 5 if the reaction was pseudo-first order.

Elucidating  $k_{\rm r,1}$  and  $k_{\rm m}$  for plasma degradation requires additional experiments. Here, we demonstrate that changing the plasma current, which affects the intrinsic surface reaction rate, can help decouple  $k_{\rm r,1}$  from  $k_{\rm m}$ . Figure 5 shows both  $X_{\rm D}$ 

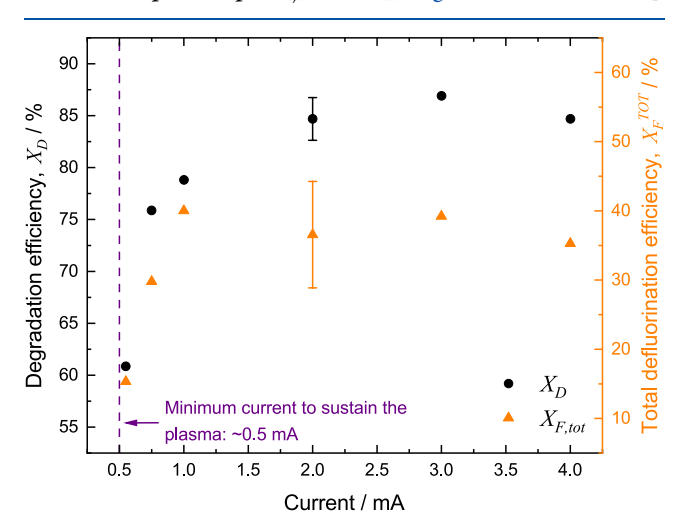


**Figure 5.** PFOA degradation and defluorination efficiency as a function of plasma current. Data were collected at the end of 1 h treatments.

and  $X_{\rm F}^{\rm TOT}$ , as a function of current for 1 h of treatment. The current range was limited between 0.55 and 4 mA. Below 0.5

mA, a plasma could not be sustained, whereas above 4 mA, the plasma electrode became exceedingly hot, as can be inferred from the visible blackbody radiation emitted from the tip of the electrode. Both  $X_{\rm D}$  and  $X_{\rm F}^{\rm TOT}$  are seen to approximately saturate at 2 mA ( $\sim$ 1 A/cm² current density, 50 times greater than that of the BDD). Therefore, any additional current above 2 mA is almost entirely wasted, in agreement with the increasing energy yield with decreasing current shown in Figure 4a. Hence, at and above 2 mA, the process is expected to be entirely mass transfer limited. When  $k_{\rm r,1} \gg k_{\rm m}$ , eq 5 reduces to

$$\frac{X_{\rm D,1}}{100} \cong 1 - \exp\left(-\frac{A_{\rm s}}{V_{\rm liq}}k_{\rm m}t\right) \tag{7}$$

Note that  $A_{\rm s}/V_{\rm liq}$  is the interfacial area concentration; therefore,  $k_{\rm m}A_{\rm s}/V_{\rm liq}$  is equivalent to  $k_{\rm La}$ , known as the volumetric mass transfer coefficient. Using eq 7,  $k_{\rm m}$  can be expressed explicitly:

$$k_{\rm m} \cong -\frac{V_{\rm liq}}{A_{\rm s}t} \ln \left(1 - \frac{X_{\rm D,1}}{100}\right)$$
 (8)

From the single data point collected at 3 mA (Figure 5) at the end of a 1 h long treatment,  $k_{\rm m}$  was estimated to be 0.058 m/s. By using this value in eq 7, the entire time trend of  $X_D$ was captured accurately at a different current, 2 mA, at which the degradation is still mass transfer limited (Figure S6). For the validity of this mass transfer coefficient, an additional check can be done by comparing the rates of mass transfer and degradation rates in the case of the BDD electrode. The general expression for the mass transfer coefficient derived from similarity arguments shows the following proportionality:  $k_{\rm m} \propto L_{\rm c} Re^{\rm p} Sc^{\rm q}$ , where  $L_{\rm c}$  is the characteristic size, Re is the Reynolds number, Sc is the Schmidt number, and p and q are constants. Since the same cell and flow conditions are used for both electrodes, and since the characteristic dimensions of the BDD electrode are similar to the size of the plasma-liquid interface, at least some of the local mass transfer coefficients for the BDD are expected to be close to the overall value estimated for the plasma electrode. Assuming that the value of  $k_{
m m}$  estimated above applies to the BDD electrode, the mass transfer rate to the BDD at the beginning of the process,  $k_{\rm m}C_{\rm p0}$ , is equal to  $1.2 \times 10^{-3}$  mol/m<sup>2</sup>s. This value is more than 1000times larger than the rate of degradation for the BDD, given by the intrinsic zero-order rate constant,  $k_{r,0}$ , which is selfconsistent with the kinetically limited degradation process observed with the BDD electrode.

Role of the Counter Electrode. Despite the significant differences in the mechanism and structure of the plasma and BDD working electrodes, both approaches need a counter electrode during operation for PFOA degradation. There are relatively few studies of the effect of the counter electrode on PFAS degradation. Costa et al. showed that when a BDD serves as the anode, a Pt cathode yields the highest degradation

Table 1. Efficiencies in the Single and Split Cells

	$X_{ m D}/\%$		$X_{ m F}/\%$		$X_{\rm F}^{ m TOT}/\%$	
	single cell	split cell	single cell	split cell	single cell	split cell
plasma (–) 1 h run	$84.7 \pm 2.1$	$58.5 \pm 2.8$	$43.1 \pm 8.4$	$59.3 \pm 2.2$	$36.6 \pm 7.7$	$34.7 \pm 3.0$
BDD (+) 2 h run	$38.3 \pm 0.6$	$59.8 \pm 0.9$	$44.4 \pm 17.3$	$40.5 \pm 5.6$	$16.9 \pm 6.3$	$24.2 \pm 3.4$

and defluorination efficiencies as compared to BDD, Zr, and stainless steel.<sup>39</sup> Here, we carried out PFAS degradation in a split cell with a cation exchange membrane to decouple the cathodic and anodic processes, to determine if the counter electrode plays any role. For the split-cell experiments, the same sample volume and concentration were used in the cell of the working electrode as in the single-cell experiments, but the cell of the counter electrode contained no PFOA at the beginning of the process. As shown in Table 1, for a plasma electrode,  $X_D$  decreased by almost 30% in a split cell, a change that is not expected from mass transfer rates. This drop was accompanied by approximately a 10% increase in  $X_{\rm F}$ , which resulted in  $X_F^{\text{TOT}}$  values being similar to values obtained in the single cell. Therefore, the counter electrode appears to play a role in the degradation and defluorination processes for a plasma electrode, perhaps by reoxidation of the free fluoride in the latter case. In contrast, for the BDD electrode,  $X_D$  increased in the split cell, whereas  $X_F$  did not change appreciably. The reason for the increase in degradation efficiency is unclear. One possibility is that there is a species generated at the counter electrode, which interferes with PFOA degradation. In the case of the plasma as the working electrode, most of the degradation and defluorination are clearly induced by the plasma.

Split cell results indicate that the plasma should ideally be paired with an anode, which is synergistically capable of degradation and defluorination. The asymmetric nature of the electrode performance shown in Figure 2 suggests that the BDD is a potential anode for the plasma cathode. This electrode combination was used for PFOA degradation in a single cell at a current of 2 mA, chosen to establish a comparison with the data shown in Figure 2a. The results indicated no significant improvement in the degradation performance, but an approximately 10% increase in  $X_{\rm F}^{\rm TOT}$ was obtained (Figure S7). These results hint that 2 mA may correspond to too low of a current density (4 mA/cm<sup>2</sup>) and reaction rate for the BDD, and in the future, electrodes must be designed with better matching of power density. That is, either smaller areas for the BDD or, preferably, larger currents spread over a large area for the plasma are needed. 52

Role of Short-Lived Reactive Species. Although the split cell experiments indicated that both working electrodes can effectively degrade PFOA, where the plasma is assisted by the counter electrode, additional experiments are necessary for comparing major degradation pathways. Mechanistic insight has been obtained for plasma-liquid experiments by using radical scavengers. 45,64,68-70 Radical scavengers can rapidly react with a potential reaction intermediate with relatively high specificity. Observing a change in the figures of merit associated with PFOA removal, in the presence of a scavenger, indicates whether the targeted radical participates in the reaction. A likely reducing species is solvated electrons, and a likely oxidizing species is hydroxyl radicals (OH), and thus NaNO3 and NaTA were selected as the respective radical scavengers. OH radicals are expected to be produced by both the plasma<sup>69,71</sup> and BDD electrodes, but solvated electrons are specific to the plasma, <sup>64</sup> especially for a cathodic continuous DC plasma.

Upon adding a 10 mM concentration of the OH scavenging NaTA,  $X_D$  for the plasma electrode slightly increased, but the efficiency of the BDD electrode dropped sharply (Figure 6). The results for the BDD electrode confirm that OH radicals,

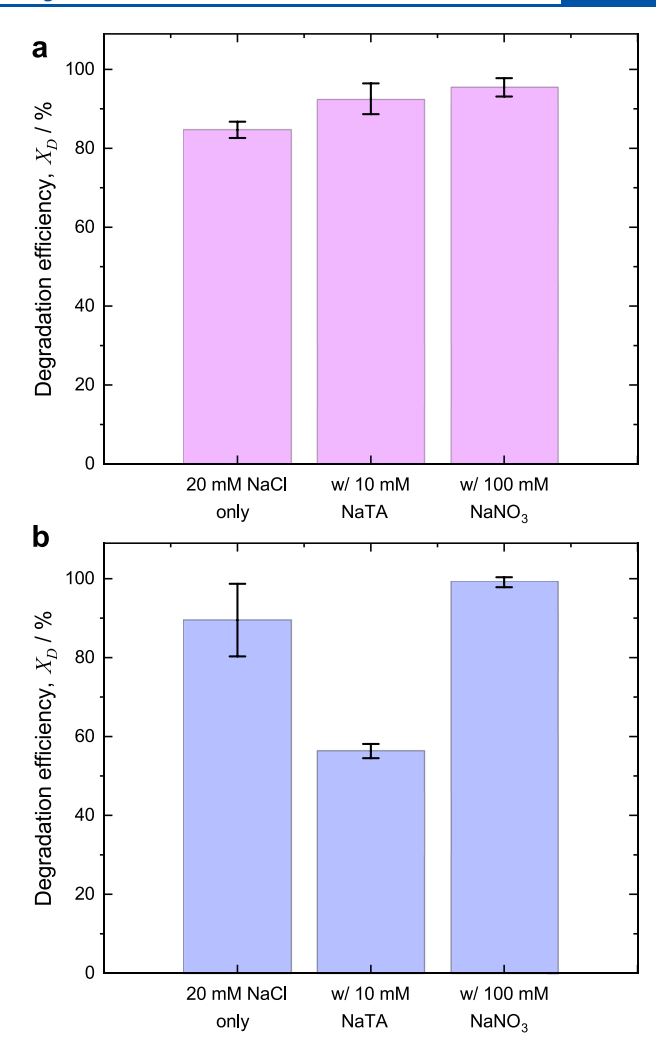


**Figure 6.** PFOA degradation efficiency with and without radical scavengers. (a) Plasma electrode as the cathode; (b) BDD electrode as the anode. In addition to the scavenger, 20 mM NaCl was present in all solutions as the background electrolyte. Experiments with the plasma electrode were conducted at 2 mA for 1 h duration. Experiments involving the BDD were 5 h long.

which have been previously suspected to be generated with a BDD electrode,  $^{38,61,72}$  are partially responsible for PFOA degradation. Interestingly, we confirmed that OH radicals were produced by an anodic plasma, as quantified by 0.24  $\mu\rm M$  HTA formed after 2 h of treatment at 2 mA, and yet led to very little PFOA degradation (see Figure 2a). Previous studies have shown that free OH cannot degrade PFOA,  $^{8,9}$  and the mechanism in the case of a BDD electrode is a surface-mediated process.  $^{73}$ 

The rate of OH formation was found to correlate directly with and explain the polarity dependence of degradation for a BDD electrode. An anodic BDD produced approximately 0.1  $\mu$ M HTA after a 5 h long treatment, whereas a cathodic BDD produced approximately 6 times less. Since the concentration of NaTA was 500 times more than the initial concentration of PFOA, NaTA was more abundant than PFOA nearby the BDD surface. Assuming that NaTA captures the majority of the physisorbed OH, the remaining degradation capability of the BDD can be associated with direct electron transfer<sup>62</sup> and oxidation through reversible surface oxides.<sup>74</sup>

In the presence of a 100 mM concentration of the solvated electron scavenging NaNO<sub>3</sub>, the plasma electrode showed a minor increase in  $X_{\rm D}$ , whereas the BDD electrode showed only a negligible change in the efficiency. While NaNO<sub>3</sub> could be mass transfer limited due to the adverse electric fields for the NO<sub>3</sub><sup>-</sup> anion near the plasma—liquid interface, 100 mM has been previously shown to be sufficient to quench the majority of the solvated electrons. <sup>64,70,75</sup> The absence of a clear decrease in degradation performance for either scavenger suggests that PFOA degradation with the plasma electrode is not radical-mediated.

The slight increase in  $X_{\rm D}$  for the plasma electrode in our experiments with a radical scavenger may be related to the salting out effect of PFOA. An increasing amount of the total dissolved solids (TDS) decreases the surface tension, which leads to an increase in the surface excess of PFOA at the interface. Higher surface excess allows an increased probability for direct interaction with the gaseous electrons in the plasma above the interface. Similar findings were presented in a recent report, where an increase in the observed rate constant was measured due to higher surface accumulation with increasing solution conductivity.

A Simple Reaction Expression for Plasma Degradation. Based on experiments with the split cell and radical scavengers and the evidence of surface excess of PFOA playing a role in degradation, we suggest that degradation in a cathodic plasma occurs through an Eley-Rideal (ER) type mechanism at the plasma-liquid interface. In an ER mechanism, one of the reactants of a bimolecular surface reaction reacts directly from the gas phase, which we suggest could be the gaseous electrons in the anode sheath of the plasma. These electrons can interact with the hydrophobic tail of PFOA, which protrudes upward and away from the water surface.<sup>78</sup> The slight decrease in defluorination rates over time (Figure 2c) may be the result of transport limitations or the formation of shorter-chain PFAS, which have lower surface activity, thus lowering the surface concentration. Thagard and co-workers have presented a similar argument,<sup>53</sup> and they have recently mentioned the major role of mass transport in plasma-based water treatment. However, a simple quantitative model that explains interplay of reaction kinetics, mass transport, and surface accumulation during plasma degradation of PFAS in a well-mixed environment is lacking. The film model that we presented can be modified to include all these mechanisms in a quantitative manner, along with incorporating the direct interaction of PFOA with gaseous electrons at the plasmawater interface.

The ER hypothesis allows closure of the film model for plasma degradation, where we had previously assumed a generic first-order reaction, which cannot explain the increase in degradation efficiency with increasing current (Figure 5). A more general ER mechanism that describes the degradation rate at a plasma—liquid interface is

$$r_{\rm p} = -k_{\rm r}^{\Box} \theta C_{\rm e}^{\rm m} \tag{9}$$

where  $k_r^{\square}$  is the intrinsic rate constant,  $\theta$  is the surface coverage of PFOA, and  $C_e$  is the gaseous electron concentration at the edge of the anode sheath (see the Supplementary Information for the full derivation). The power m stands for nonelementary pathways and denotes the possibility of more than one electron being involved in the degradation of a single PFOA molecule. Surface coverage is

expressed as the ratio of the concentration on the surface,  $C_{\rm ps}$ , and the maximum surface excess,  $\Gamma_{\rm max}$ :  $\theta = C_{\rm ps}/\Gamma_{\rm max}$ . Both concentrations have units of moles/area. The value of  $\Gamma_{\rm max}$  was measured to be approximately 1.23 mM/m², independent of the TDS content. Using  $\Gamma_{\rm max}$  the Langmuir–Szyszkowski equation can be used to describe the partitioning of PFOA on the water surface:  $^{80}$ 

$$C_{\rm ps} = \Gamma_{\rm max} \frac{C_{\rm p}^{\ *}}{C_{\rm p}^{\ *} + b} \tag{10}$$

where  $C_{\rm p}^{*}$  is the volumetric concentration just beneath the interface, and b is the surface activity, which depends on the TDS content as  $^{76}$  20.7 × TDS $^{-0.15}$  in  $\mu$ M. For a 20 mM NaCl solution, TDS = 1169 mg/L, and thus, for our experiments, b = 7.2  $\mu$ M. This information allows us to write  $\theta$  in terms of the known parameters and  $C_{\rm p}^{*}$ , a parameter in the film model (see Supplementary Information). Given the fact that the plasma electrode operates in a mass transfer-limited regime, and since the initial PFOA concentration is of the same order of magnitude as b, it is expected that  $C_{\rm p}^{*} \ll b$ . Hence, eq 9 reduces to

$$r_{\rm p} \cong -\frac{k_{\rm r}}{b} C_{\rm p}^* C_{\rm e}^{\rm m} \tag{11}$$

Eq 11 shows that the reaction rate increases with increasing TDS, due to a decrease in b, and increases with  $C_{\rm e}$ , which is proportional to current. Furthermore, the rate expression is pseudo first-order since  $C_{\rm e}$  and b do not change during degradation. This observation yields a definition for  $k_{\rm r,1}$  in eq 5:

$$k_{r,1} \cong \frac{k_r^{\square}}{b} C_e^{m} \tag{12}$$

While the electron concentration above the interface is not known, it can be related to current, which is a directly measured parameter. Using a drift-diffusion model yields the following expression for  $C_{\rm e}$  (see Supplementary Information):

$$C_{\rm e} = \frac{I}{A_{\rm s}F} \frac{1}{\frac{\mu_{\rm d_a}(|V_{\rm a}| + \frac{k_{\rm B}T_{\rm e}}{l_{\rm e}})}{1}}$$
(13)

In eq 11, I is the current,  $\mu_{\rm e}$  is the electron mobility,  $|V_{\rm a}|$  is the mean potential in the anode sheath,  $d_{\rm a}$  is the width of the anode sheath,  $k_{\rm B}$  is Boltzmann's constant, and  $T_{\rm e}$  is the mean electron temperature in the anode sheath.  $\mu_{\rm e}$  can be calculated from known relationships, <sup>81</sup> and  $|V_{\rm a}|$  and  $T_{\rm e}$  are estimated from a recent multiphase simulation of the plasma—liquid interface beneath a DC plasma cathode, <sup>75</sup> allowing the calculation of  $C_{\rm e}$  as a function of current (see Supplementary Information). Eq 13 allows determination of the intrinsic rate constant,  $k_{\rm r}$ , from the data presented in Figure 5.

Nonlinear regression of eq 5 combined with eqs 12 and 13 to the degradation data yields the three fitting curves in Figure 7. For m=1, the  $k_r^{\square}$  has a simple physical meaning with the units of numbers of PFOA molecules degraded per volumetric interfacial area per electron per time, and is found to be 443 m s<sup>-1</sup>. However, the m=1 description yields a poor fit. For m=2, a satisfactory fit to experimental data was obtained, and the value of the intrinsic rate constant  $k_r^{\square}$  is found to be 2.89 ×  $10^8$  m<sup>4</sup> mol<sup>-1</sup> s<sup>-1</sup> (see Table S4 for a list of rate constants

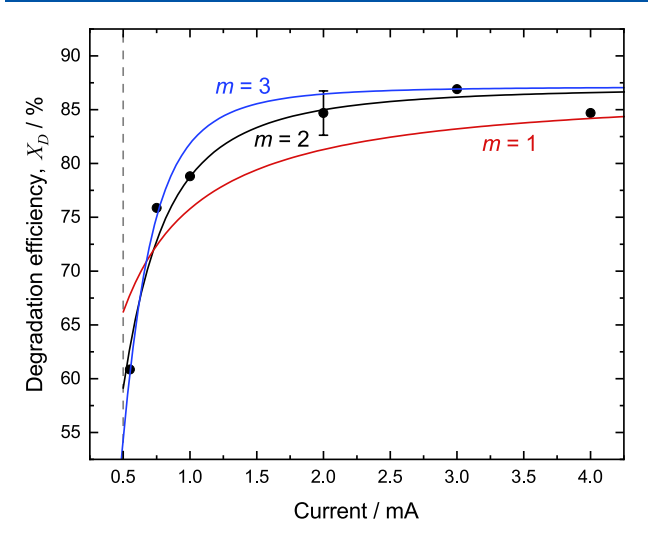


**Figure 7.** Fits to degradation vs current data for the cathodic plasma. m is the order for the gaseous electron concentration in eq 9 and was changed to obtain the best fit and to estimate the intrinsic reaction rate constant,  $k_{\rm r}^{\Box}$ .

obtained in this study). Regression using a higher integer value for the order of electron concentration reduced the accuracy of the fit (Figure 7). By interpreting the value of m as the number of electrons involved in the degradation of a PFOA molecule, the faradaic efficiency,

$$\eta_{\rm F} = \frac{2FV_{\rm liq}C_{\rm p0}X_{\rm D,1}}{I\ t} \tag{14}$$

where F is Faraday's constant, can also be estimated. For the lowest current employed, I=0.55 mA, the highest time-averaged faradaic efficiency obtained was 2.4%.  $\eta_{\rm F}$  is usually difficult to calculate in plasma systems and has not been reported. The value is higher than conventional electrochemical degradation with  $C_{\rm p0} \geq 20~\mu{\rm M}$ , which are rarely above 0.1% (Table S2).

#### CONCLUSIONS

Our comparative study of the plasma and BDD electrodes showed that while these two approaches differ significantly in terms of reaction rates and mechanisms, they can have surprisingly similar energy efficiencies. While the BDD anode is capable of degrading and defluorinating PFAS, it was found that the plasma electrode can remove PFOA with a similar efficiency only when operated as the cathode. Both electrodes produce OH radicals, but OH radicals are only effective in the case of the BDD because they likely are more reactive when bound to the anode surface. Degradation by a plasma does not involve any of the aqueous radicals investigated in this work, OH radicals and solvated electrons but appears to rely on direct reaction with gaseous electrons, suggesting an ER-type mechanism. The plasma has very high surface-specific rates, predominantly because of high local current densities, and thus, its performance is controlled by mass transfer. This result indicates that plasmas can be very efficient at high contaminant concentrations, but for dilute systems, its efficiency is limited. Therefore, to increase efficiency, a significant preconcentration of PFAS streams is needed. On the other hand, for the BDD, mass transfer limitations do not appear, and steady, albeit lower, rates of defluorination are possible. The counter electrode plays a role in both cases, but for the BDD, it reduces degradation and for the plasma, it increases degradation. In the future, it may be possible to engineer a system that combines both the plasma and the BDD electrodes to achieve synergistic effects, but the very different power inputs and reaction-transport effects must be addressed.

#### ASSOCIATED CONTENT

#### Supporting Information

The Supporting Information is available free of charge at https://pubs.acs.org/doi/10.1021/acs.langmuir.2c01227.

Calibration of the NaTA fluorescence assay, LC/MS operational parameters, cell voltage measurements, first-order fit to cathodic plasma degradation, calculation of Ohmic losses, definitions of the performance metrics, literature review tables on electrochemical and plasma degradation, derivation of the film model of mass transfer with chemical reaction, mass-transfer-limited degradation for the plasma electrode, asymmetric degradation, estimation of gaseous electron concentration nearby the interface, and list of rate constants (PDF)

#### AUTHOR INFORMATION

#### **Corresponding Authors**

Xiao Su — Department of Chemical and Biomolecular Engineering, University of Illinois at Urbana-Champaign, Urbana 61801 Illinois, United States; ocid.org/0000-0001-7794-290X; Phone: +1 (217) 300-0134; Email: x2su@illinois.edu

R. Mohan Sankaran — Department of Nuclear, Plasma and Radiological Engineering, University Illinois at Urbana-Champaign, Urbana 61801 Illinois, United States; orcid.org/0000-0002-9399-4790; Phone: +1 (217) 244-7316; Email: rmohan@illinois.edu

#### **Authors**

Necip B. Üner — Department of Nuclear, Plasma and Radiological Engineering, University Illinois at Urbana-Champaign, Urbana 61801 Illinois, United States; Chemical Engineering Department, Middle East Technical University, Ankara 06800, Turkey; orcid.org/0000-0002-5719-6417

Paola Baldaguez Medina — Department of Chemical and Biomolecular Engineering, University of Illinois at Urbana-Champaign, Urbana 61801 Illinois, United States

Jasmine L. Dinari — Department of Nuclear, Plasma and Radiological Engineering, University Illinois at Urbana-Champaign, Urbana 61801 Illinois, United States;

Complete contact information is available at: https://pubs.acs.org/10.1021/acs.langmuir.2c01227

orcid.org/0000-0001-5652-2383

#### Notes

The authors declare no competing financial interest.

#### ACKNOWLEDGMENTS

N.B.Ü. and R.M.S. acknowledge support from the Air Force Office of Scientific Research under Grant No. FA9550-19-1-0088. P.B.M. acknowledges support from the National Science Foundation Graduate Research Fellowship Program under Grant No. DGE 21-46756. X.S. acknowledges support from National Science Foundation Grant #1931941. J.L.D. acknowledges support from the Henry Luce Foundation.

#### ABBREVIATIONS

PFAS per- and polyfluoro alkyl substances

PFOA perfluorooctanoic acid BDD boron-doped diamond

DC direct current

LC-MS liquid chromatography-mass spectrometry

NaTA disodium terephthalate HTA 2-hydroxyterephthalic acid TDS total dissolved solids

ER Eley-Rideal

#### REFERENCES

- (1) National Cancer Institute. PFAS Exposure and Risk of Cancer.
- (2) Wielsøe, M.; Long, M.; Ghisari, M.; Bonefeld-Jørgensen, E. C. Perfluoroalkylated Substances (PFAS) Affect Oxidative Stress Biomarkers in Vitro. *Chemosphere* **2015**, *129*, 239–245.
- (3) Temkin, A. M.; Hocevar, B. A.; Andrews, D. Q.; Naidenko, O. V.; Kamendulis, L. M. Application of the Key Characteristics of Carcinogens to Per and Polyfluoroalkyl Substances. *Int. J. Environ. Res. Public Health* **2020**, *17*, 1668.
- (4) Fenton, S. E.; Ducatman, A.; Boobis, A.; DeWitt, J. C.; Lau, C.; Ng, C.; Smith, J. S.; Roberts, S. M. Per- and Polyfluoroalkyl Substance Toxicity and Human Health Review: Current State of Knowledge and Strategies for Informing Future Research. *Environ. Toxicol. Chem.* **2021**, *40*, 606–630.
- (5) Li, Y.; Fletcher, T.; Mucs, D.; Scott, K.; Lindh, C. H.; Tallving, P.; Jakobsson, K. Half-Lives of PFOS, PFHxS and PFOA after End of Exposure to Contaminated Drinking Water. *Occup. Environ. Med.* **2018**, 75, 46–51.
- (6) Huheey, J. E.; Keiter, E. A.; Keiter, R. L. *Inorganic Chemistry: Principles of Structure and Reactivity*, 4th ed.; HarperCollins College Publishers: New York, NY, 1993.
- (7) Zhuo, Q.; Deng, S.; Yang, B.; Huang, J.; Wang, B.; Zhang, T.; Yu, G. Degradation of Perfluorinated Compounds on a Boron-Doped Diamond Electrode. *Electrochim. Acta* **2012**, *77*, 17–22.
- (8) Moriwaki, H.; Takagi, Y.; Tanaka, M.; Tsuruho, K.; Okitsu, K.; Maeda, Y. Sonochemical Decomposition of Perfluorooctane Sulfonate and Perfluorooctanoic Acid. *Environ. Sci. Technol.* **2005**, *39*, 3388–3392.
- (9) Schröder, H. F.; Meesters, R. J. W. Stability of Fluorinated Surfactants in Advanced Oxidation Processes—A Follow up of Degradation Products Using Flow Injection—Mass Spectrometry, Liquid Chromatography—Mass Spectrometry and Liquid Chromatography—Multiple Stage Mass Spectrometry. *J. Chromatogr. A* 2005, 1082, 110–119.
- (10) Nzeribe, B. N.; Crimi, M.; Thagard, S. M.; Holsen, T. M. Physico-Chemical Processes for the Treatment of Per-And Polyfluoroalkyl Substances (PFAS): A Review. *Crit. Rev. Environ.* **2019**, 28, 753–754.
- (11) Horst, J.; McDonough, J.; Ross, I.; Dickson, M.; Miles, J.; Hurst, J.; Storch, P. Water Treatment Technologies for PFAS: The Next Generation. *Groundwater Monit. Rem.* **2018**, 38, 13–23.
- (12) Takagi, S.; Adachi, F.; Miyano, K.; Koizumi, Y.; Tanaka, H.; Watanabe, I.; Tanabe, S.; Kannan, K. Fate of Perfluorooctanesulfonate and Perfluorooctanoate in Drinking Water Treatment Processes. *Water Res.* **2011**, *45*, 3925–3932.
- (13) Park, M.; Wu, S.; Lopez, I. J.; Chang, J. Y.; Karanfil, T.; Snyder, S. A. Adsorption of Perfluoroalkyl Substances (PFAS) in Groundwater by Granular Activated Carbons: Roles of Hydrophobicity of PFAS and Carbon Characteristics. *Water Res.* **2020**, *170*, No. 115364.
- (14) Gagliano, E.; Sgroi, M.; Falciglia, P. P.; Vagliasindi, F. G. A.; Roccaro, P. Removal of Poly- and Perfluoroalkyl Substances (PFAS) from Water by Adsorption: Role of PFAS Chain Length, Effect of Organic Matter and Challenges in Adsorbent Regeneration. *Water Res.* 2020, 171, No. 115381.

- (15) Dixit, F.; Dutta, R.; Barbeau, B.; Berube, P.; Mohseni, M. PFAS Removal by Ion Exchange Resins: A Review. *Chemosphere* **2021**, *272*, No. 129777.
- (16) Woodard, S.; Berry, J.; Newman, B. Ion Exchange Resin for PFAS Removal and Pilot Test Comparison to GAC. *Rem. J.* **2017**, *27*, 19–27.
- (17) Tang, C. Y.; Fu, Q. S.; Robertson, A. P.; Criddle, C. S.; Leckie, J. O. Use of Reverse Osmosis Membranes to Remove Perfluorooctane Sulfonate (PFOS) from Semiconductor Wastewater. *Environ. Sci. Technol.* **2006**, *40*, 7343–7349.
- (18) Mastropietro, T. F.; Bruno, R.; Pardo, E.; Armentano, D. Reverse Osmosis and Nanofiltration Membranes for Highly Efficient PFASs Removal: Overview, Challenges and Future Perspectives. *Dalton Trans.* **2021**, *50*, 5398–5410.
- (19) Robey, N. M.; da Silva, B. F.; Annable, M. D.; Townsend, T. G.; Bowden, J. A. Concentrating Per- and Polyfluoroalkyl Substances (PFAS) in Municipal Solid Waste Landfill Leachate Using Foam Separation. *Environ. Sci. Technol.* **2020**, *54*, 12550–12559.
- (20) Burns, D. J.; Stevenson, P.; Murphy, P. J. C. PFAS Removal from Groundwaters Using Surface-Active Foam Fractionation. *Rem. J.* **2021**, *31*, 19–33.
- (21) McCleaf, P.; Kjellgren, Y.; Ahrens, L. Foam Fractionation Removal of Multiple Per- and Polyfluoroalkyl Substances from Landfill Leachate. *AWWA Water Sci.* **2021**, *3*, No. e1238.
- (22) Kim, K.; Baldaguez Medina, P.; Elbert, J.; Kayiwa, E.; Cusick, R. D.; Men, Y.; Su, X. Molecular Tuning of Redox-Copolymers for Selective Electrochemical Remediation. *Adv. Funct. Mater.* **2020**, *30*, No. 2004635.
- (23) Medina, P. B.; Cotty, S.; Kim, K.; Elbert, J.; Su, X. Emerging Investigator Series: Electrochemically-Mediated Remediation of GenX Using Redox-Copolymers. *Environ. Sci.: Water Res. Technol.* **2021**, *7*, 2231–2240.
- (24) Román Santiago, A.; Baldaguez Medina, P.; Su, X. Electrochemical Remediation of Perfluoroalkyl Substances from Water. *Electrochim. Acta* **2022**, 403, No. 139635.
- (25) Singh Kalra, S.; Cranmer, B.; Dooley, G.; Hanson, A. J.; Maraviov, S.; Mohanty, S. K.; Blotevogel, J.; Mahendra, S. Sonolytic Destruction of Per- and Polyfluoroalkyl Substances in Groundwater, Aqueous Film-Forming Foams, and Investigation Derived Waste. *Chem. Eng. J.* **2021**, *425*, No. 131778.
- (26) Cao, H.; Zhang, W.; Wang, C.; Liang, Y. Sonochemical Degradation of Poly- and Perfluoroalkyl Substances A Review. *Ultrason. Sonochem.* **2020**, *69*, No. 105245.
- (27) Hori, H.; Hayakawa, E.; Einaga, H.; Kutsuna, S.; Koike, K.; Ibusuki, T.; Kiatagawa, H.; Arakawa, R. Decomposition of Environmentally Persistent Perfluorooctanoic Acid in Water by Photochemical Approaches. *Environ. Sci. Technol.* **2004**, *38*, 6118–6124.
- (28) Hori, H.; Yamamoto, A.; Hayakawa, E.; Taniyasu, S.; Yamashita, N.; Kutsuna, S.; Kiatagawa, H.; Arakawa, R. Efficient Decomposition of Environmentally Persistent Perfluorocarboxylic Acids by Use of Persulfate as a Photochemical Oxidant. *Environ. Sci. Technol.* **2005**, *39*, 2383–2388.
- (29) Park, H.; Vecitis, C. D.; Cheng, J.; Choi, W.; Mader, B. T.; Hoffmann, M. R. Reductive Defluorination of Aqueous Perfluorinated Alkyl Surfactants: Effects of Ionic Headgroup and Chain Length. *J. Phys. Chem. A* **2009**, *113*, 690–696.
- (30) Lin, H.; Niu, J.; Ding, S.; Zhang, L. Electrochemical Degradation of Perfluorooctanoic Acid (PFOA) by Ti/SnO2–Sb, Ti/SnO2–Sb/PbO2 and Ti/SnO2–Sb/MnO2 Anodes. *Water Res.* **2012**, *46*, 2281–2289.
- (31) Lin, H.; Niu, J.; Xu, J.; Huang, H.; Li, D.; Yue, Z.; Feng, C. Highly Efficient and Mild Electrochemical Mineralization of Long-Chain Perfluorocarboxylic Acids (C9–C10) by Ti/SnO2–Sb–Ce, Ti/SnO2–Sb/Ce–PbO2, and Ti/BDD Electrodes. *Environ. Sci. Technol.* 2013, 47, 13039–13046.
- (32) Schaefer, C. E.; Andaya, C.; Burant, A.; Condee, C. W.; Urtiaga, A.; Strathmann, T. J.; Higgins, C. P. Electrochemical Treatment of Perfluorooctanoic Acid and Perfluorooctane Sulfonate: Insights into

- Mechanisms and Application to Groundwater Treatment. *Chem. Eng. J.* **2017**, *317*, 424–432.
- (33) Barisci, S.; Suri, R. Electrooxidation of Short and Long Chain Perfluorocarboxylic Acids Using Boron Doped Diamond Electrodes. Chemosphere 2020, 243, No. 125349.
- (34) Gomez-Ruiz, B.; Diban, N.; Urtiaga, A. Comparison of Microcrystalline and Ultrananocrystalline Boron Doped Diamond Anodes: Influence on Perfluorooctanoic Acid Electrolysis. *Sep. Purif. Technol.* **2019**, 208, 169–177.
- (35) Sukeesan, S.; Boontanon, N.; Boontanon, S. K. Improved Electrical Driving Current of Electrochemical Treatment of Per- and Polyfluoroalkyl Substances (PFAS) in Water Using Boron-Doped Diamond Anode. *Environ. Technol. Innovation* **2021**, 23, No. 101655.
- (36) Trautmann, A. M.; Schell, H.; Schmidt, K. R.; Mangold, K.-M.; Tiehm, A. Electrochemical Degradation of Perfluoroalkyl and Polyfluoroalkyl Substances (PFASs) in Groundwater. *Water Sci. Technol.* **2015**, *71*, 1569–1575.
- (37) Zhuo, Q.; Deng, S.; Yang, B.; Huang, J.; Yu, G. Efficient Electrochemical Oxidation of Perfluorooctanoate Using a Ti/SnO2-Sb-Bi Anode. *Environ. Sci. Technol.* **2011**, *45*, 2973–2979.
- (38) Urtiaga, A.; Fernández-González, C.; Gómez-Lavín, S.; Ortiz, I. Kinetics of the Electrochemical Mineralization of Perfluorooctanoic Acid on Ultrananocrystalline Boron Doped Conductive Diamond Electrodes. *Chemosphere* **2015**, *129*, 20–26.
- (39) Garcia-Costa, A. L.; Savall, A.; Zazo, J. A.; Casas, J. A.; Groenen Serrano, K. On the Role of the Cathode for the Electro-Oxidation of Perfluorooctanoic Acid. *Catalysts* **2020**, *10*, 902.
- (40) Pierpaoli, M.; Szopińska, M.; Wilk, B. K.; Sobaszek, M.; Łuczkiewicz, A.; Bogdanowicz, R.; Fudala-Książek, S. Electrochemical Oxidation of PFOA and PFOS in Landfill Leachates at Low and Highly Boron-Doped Diamond Electrodes. *J. Hazard. Mater.* **2021**, 403, No. 123606.
- (41) Xiao, H.; Lv, B.; Zhao, G.; Wang, Y.; Li, M.; Li, D. Hydrothermally Enhanced Electrochemical Oxidation of High Concentration Refractory Perfluorooctanoic Acid. *J. Phys. Chem. A* **2011**, *115*, 13836–13841.
- (42) Barisci, S.; Suri, R. Electrooxidation of Short- and Long-Chain Perfluoroalkyl Substances (PFASs) under Different Process Conditions. *J. Environ. Chem. Eng.* **2021**, *9*, No. 105323.
- (43) Obo, H.; Takeuchi, N.; Yasuoka, K. Decomposition of Perfluorooctanoic Acid in Water Using Multiple Plasma Generation. *IEEE Trans. Plasma Sci.* **2013**, *41*, 3634–3639.
- (44) Takeuchi, N.; Kitagawa, Y.; Kosugi, A.; Tachibana, K.; Obo, H.; Yasuoka, K. Plasma—Liquid Interfacial Reaction in Decomposition of Perfluoro Surfactants. J. Phys. D: Appl. Phys. 2013, 47, No. 045203.
- (45) Stratton, G. R.; Dai, F.; Bellona, C. L.; Holsen, T. M.; Dickenson, E. R. V.; Mededovic Thagard, S. Plasma-Based Water Treatment: Efficient Transformation of Perfluoroalkyl Substances in Prepared Solutions and Contaminated Groundwater. *Environ. Sci. Technol.* 2017, *51*, 1643–1648.
- (46) Mahyar, A.; Miessner, H.; Mueller, S.; Hama Aziz, K. H.; Kalass, D.; Moeller, D.; Kretschmer, K.; Robles Manuel, S.; Noack, J. Development and Application of Different Non-Thermal Plasma Reactors for the Removal of Perfluorosurfactants in Water: A Comparative Study. *Plasma Chem. Plasma Process.* **2019**, 39, 531–544.
- (47) Lewis, A. J.; Joyce, T.; Hadaya, M.; Ebrahimi, F.; Dragiev, I.; Giardetti, N.; Yang, J.; Fridman, G.; Rabinovich, A.; Fridman, A. A.; et al. Rapid Degradation of PFAS in Aqueous Solutions by Reverse Vortex Flow Gliding Arc Plasma. *Environ. Sci.: Water Res. Technol.* **2020**, *6*, 1044–1057.
- (48) Saleem, M.; Biondo, O.; Sretenović, G.; Tomei, G.; Magarotto, M.; Pavarin, D.; Marotta, E.; Paradisi, C. Comparative Performance Assessment of Plasma Reactors for the Treatment of PFOA; Reactor Design, Kinetics, Mineralization and Energy Yield. *Chem. Eng. J.* **2020**, 382, No. 123031.
- (49) Wang, X.; Wang, P.; Liu, X.; Hu, L.; Wang, Q.; Xu, P.; Zhang, G. Enhanced Degradation of PFOA in Water by Dielectric Barrier Discharge Plasma in a Coaxial Cylindrical Structure with the

- Assistance of Peroxymonosulfate. Chem. Eng. J. 2020, 389, No. 124381.
- (50) Singh, R. K.; Fernando, S.; Baygi, S. F.; Multari, N.; Thagard, S. M.; Holsen, T. M. Breakdown Products from Perfluorinated Alkyl Substances (PFAS) Degradation in a Plasma-Based Water Treatment Process. *Environ. Sci. Technol.* **2019**, *53*, 2731–2738.
- (51) Palma, D.; Papagiannaki, D.; Lai, M.; Binetti, R.; Sleiman, M.; Minella, M.; Richard, C. PFAS Degradation in Ultrapure and Groundwater Using Non-Thermal Plasma. *Molecules* **2021**, *26*, 924.
- (52) Groele, J. R.; Sculley, N.; Olson, T. M.; Foster, J. E. An Investigation of Plasma-Driven Decomposition of per- and Polyfluoroalkyl Substances (PFAS) in Raw Contaminated Ground Water. *J. Appl. Phys.* **2021**, *130*, No. 053304.
- (53) Thagard, S. M.; Stratton, G. R.; Dai, F.; Bellona, C. L.; Holsen, T. M.; Bohl, D. G.; Paek, E.; Dickenson, E. R. V. Plasma-Based Water Treatment: Development of a General Mechanistic Model to Estimate the Treatability of Different Types of Contaminants. *J. Phys. D: Appl. Phys.* **2016**, *50*, No. 014003.
- (54) Swain, G. M. The Susceptibility to Surface Corrosion in Acidic Fluoride Media: A Comparison of Diamond, HOPG, and Glassy Carbon Electrodes. *J. Electrochem. Soc.* **1994**, *141*, 3382.
- (55) Gandini, D.; Maheã, E.; Michaud, P. A.; Haenni, W.; Perret, A.; Comninellis, C. Oxidation of Carboxylic Acids at Boron-Doped Diamond Electrodes for Wastewater Treatment. *J. Appl. Electrochem.* **2000**, *30*, 1345–1350.
- (56) Luong, J. H. T.; Male, K. B.; Glennon, J. D. Boron-Doped Diamond Electrode: Synthesis, Characterization, Functionalization and Analytical Applications. *Analyst* **2009**, *134*, 1965.
- (57) Pleskov, Y. V.; Sakharova, A. Y.; Krotova, M. D.; Bouilov, L. L.; Spitsyn, B. V. Photoelectrochemical Properties of Semiconductor Diamond. *J. Electroanal. Chem.* **1987**, 228, 19–27.
- (58) Niu, J.; Lin, H.; Gong, C.; Sun, X. Theoretical and Experimental Insights into the Electrochemical Mineralization Mechanism of Perfluorooctanoic Acid. *Environ. Sci. Technol.* **2013**, 47, 14341–14349.
- (59) Cha, C.; Zu, Y. Behavior of Perfluorinated Surfactants at the Electrode/Solution Interface. *Langmuir* **1998**, *14*, 6280–6286.
- (60) Fóti, G.; Gandini, D.; Comninellis, C.; Perret, A.; Haenni, W. Oxidation of Organics by Intermediates of Water Discharge on IrO2 and Synthetic Diamond Anodes. *Electrochem. Solid-State Lett.* **1999**, 2, 228–230.
- (61) Marselli, B.; Garcia-Gomez, J.; Michaud, P.-A.; Rodrigo, M. A.; Comninellis, C. Electrogeneration of Hydroxyl Radicals on Boron-Doped Diamond Electrodes. *J. Electrochem. Soc.* **2003**, *150*, D79.
- (62) Carter, K. E.; Farrell, J. Oxidative Destruction of Perfluor-ooctane Sulfonate Using Boron-Doped Diamond Film Electrodes. *Environ. Sci. Technol.* **2008**, 42, 6111–6115.
- (63) Liao, Z.; Farrell, J. Electrochemical Oxidation of Perfluorobutane Sulfonate Using Boron-Doped Diamond Film Electrodes. *J. Appl. Electrochem.* **2009**, *39*, 1993–1999.
- (64) Rumbach, P.; Bartels, D. M.; Sankaran, R. M.; Go, D. B. The Solvation of Electrons by an Atmospheric-Pressure Plasma. *Nat. Commun.* **2015**, *6*, 7248.
- (65) Rumbach, P.; Bartels, D. M.; Go, D. B. The Penetration and Concentration of Solvated Electrons and Hydroxyl Radicals at a Plasma-Liquid Interface. *Plasma Sources Sci. Technol.* **2018**, 27, 115013.
- (66) Danckwerts, P. V. Gas-Liquid Reactions; McGraw-Hill: New York, 1970.
- (67) Cussler, E. L. Diffusion: Mass Transfer in Fluid Systems, 3rd ed.; Cambridge University Press: Cambridge; New York, 2009.
- (68) Hsieh, K. C.; Wandell, R. J.; Bresch, S.; Locke, B. R. Analysis of Hydroxyl Radical Formation in a Gas-Liquid Electrical Discharge Plasma Reactor Utilizing Liquid and Gaseous Radical Scavengers. *Plasma Processes Polym.* **2017**, *14*, No. 1600171.
- (69) Shiraki, D.; Ishibashi, N.; Takeuchi, N. Quantitative Estimation of OH Radicals Reacting in Liquid Using a Chemical Probe for Plasma in Contact With Liquid. *IEEE Trans. Plasma Sci.* **2016**, 44, 3158–3163.

- (70) Hawtof, R.; Ghosh, S.; Guarr, E.; Xu, C.; Mohan Sankaran, R.; Renner, J. N. Catalyst-Free, Highly Selective Synthesis of Ammonia from Nitrogen and Water by a Plasma Electrolytic System. *Sci. Adv.*, 5, eaat5778, DOI: 10.1126/sciadv.aat5778.
- (71) Sahni, M.; Locke, B. R. Quantification of Hydroxyl Radicals Produced in Aqueous Phase Pulsed Electrical Discharge Reactors. *Ind. Eng. Chem. Res.* **2006**, *45*, 5819–5825.
- (72) Henke, A. H.; Saunders, T. P.; Pedersen, J. A.; Hamers, R. J. Enhancing Electrochemical Efficiency of Hydroxyl Radical Formation on Diamond Electrodes by Functionalization with Hydrophobic Monolayers. *Langmuir* **2019**, 35, 2153–2163.
- (73) Michaud, P.-A.; Panizza, M.; Ouattara, L.; Diaco, T.; Foti, G.; Comninellis, C. Electrochemical Oxidation of Water on Synthetic Boron-Doped Diamond Thin Film Anodes. *J. Appl. Electrochem.* **2003**, 33, 151–154.
- (74) Ogose, T.; Kasahara, S.; Ikemiya, N.; Hoshi, N.; Einaga, Y.; Nakamura, M. In Situ ATR-IR Observation of the Electrochemical Oxidation of a Polycrystalline Boron-Doped Diamond Electrode in Acidic Solutions. *J. Phys. Chem. C* **2018**, *122*, 27456–27461.
- (75) Keniley, S.; Uner, N. B.; Perez, E.; Sankaran, R. M.; Curreli, D. Multiphase Modeling of the DC Plasma-Water Interface: Application to Hydrogen Peroxide Generation with Experimental Validation. *Plasma Sources Sci. Technol.* **2022**, (in review), DOI: 10.1088/1361-6595/ac7891.
- (76) Costanza, J.; Arshadi, M.; Abriola, L. M.; Pennell, K. D. Accumulation of PFOA and PFOS at the Air–Water Interface. *Environ. Sci. Technol. Lett.* **2019**, *6*, 487–491.
- (77) Nau-Hix, C.; Holsen, T. M.; Thagard, S. M. Influence of Solution Electrical Conductivity and Ionic Composition on the Performance of a Gas—Liquid Pulsed Spark Discharge Reactor for Water Treatment. J. Appl. Phys. 2021, 130, 123301.
- (78) Ghosh, N.; Roy, S.; Mondal, J. A. On the Behavior of Perfluorinated Persistent Organic Pollutants (POPs) at Environmentally Relevant Aqueous Interfaces: An Interplay of Hydrophobicity and Hydrogen Bonding. *Langmuir* **2020**, *36*, 3720–3729.
- (79) Vasilev, M.; Conlon, P.; Bohl, D.; Thagard, S. M. The Effect of Discharge Frequency of a Gas—Liquid Plasma Reactor on Bulk Liquid Transport and Removal of Organic Contaminants. *Plasma Chem. Plasma Process.* **2022**, 42, 759.
- (80) Mededovic Thagard, S.; Stratton, G. R.; Dai, F.; Bellona, C. L.; Holsen, T. M.; Bohl, D. G.; Paek, E.; Dickenson, E. R. V. Plasma-Based Water Treatment: Development of a General Mechanistic Model to Estimate the Treatability of Different Types of Contaminants. J. Phys. D: Appl. Phys. 2017, 50, No. 014003.
- (81) Raizer, I. U. P. Gas Discharge Physics; Springer: Berlin; New York, 1997.

### ☐ Recommended by ACS

#### Perfluorooctanoic acid Degradation by UV/Chlorine

Jordin Metz, Pedro J. J. Alvarez, et al.

JULY 19, 2022

**ENVIRONMENTAL SCIENCE & TECHNOLOGY LETTERS** 

READ 🗹

# Reactive-Transport Modeling of Electrochemical Oxidation of Perfluoroalkyl Substances in Porous Flow-through Electrodes

Yusra S. Khalid, Brian P. Chaplin, et al.

FEBRUARY 17, 2022

ACS ES&T ENGINEERING

READ 🗹

## Electrochemical Transformations of Perfluoroalkyl Acid (PFAA) Precursors and PFAAs in Landfill Leachates

Vanessa Y. Maldonado, Jennifer A. Field, et al.

MARCH 17, 2022

ACS ES&T WATER

READ 🗹

#### Occurrence and Fate of Ultrashort-Chain and Other Perand Polyfluoroalkyl Substances (PFAS) in Wastewater Treatment Plants

Juhee Kim, Ching-Hua Huang, et al.

JULY 19, 2022

ACS ES&T WATER

READ 🗹

Get More Suggestions >